K. Oshima, F. Topputo, S. Campagnola, T. Yanao
Analysis of Medium-Energy Transfers to the Moon
Celestial Mechanics and Dynamical Astronomy, Vol. 127, N. 3, 2017, p. 285-300
doi:10.1007/s10569-016-9727-7

Celestial Mechanics and Dynamical Astronomy manuscript No.
(will be inserted by the editor)

Analysis of Medium-Energy Transfers to the Moon

Kenta Oshima · Francesco Topputo · Stefano Campagnola · Tomohiro Yanao

Received: date / Accepted: date

Abstract This study analyzes a recently discovered new class of exterior transfers to the Moon. These transfers terminate in retrograde ballistic capture orbits, i.e., orbits with negative Keplerian energy and angular momentum with respect to the Moon. Yet, their Jacobi constant is relatively low, for which no forbidden regions exist, and the trajectories do not appear to mimic the dynamics of the invariant manifolds of the Lagrange points. This paper shows that these orbits shadow instead lunar collision orbits.

We investigate the dynamics of singular, lunar collision orbits in the Earth–Moon planar circular restricted three-body problem, and reveal their rich phase space structure in the medium-energy regime, where invariant manifolds of the Lagrange point orbits break up. We show that lunar retrograde ballistic capture trajectories lie inside the tube structure of collision orbits. We also develop a method to compute medium-energy transfers by patching together orbits inside the collision tube and those whose apogees are located in the appropriate quadrant

K. Oshima
Ph.D. Candidate
Department of Applied Mechanics and Aerospace Engineering
Waseda University, Tokyo, 169-8555, Japan
E-mail: kenta-oshima@akane.waseda.jp

F. Topputo
Assistant Professor
Department of Aerospace Science and Technology
Politecnico di Milano, 20156, Milano, Italy
E-mail: francesco.topputo@polimi.it

S. Campagnola
Mission Analyst, International Top Young Fellow
Department of Space Flight Systems
ISAS/JAXA, Sagamihara, Kanagawa, 155-0031, Japan
E-mail: stefano.campagnola@jaxa.jp

T. Yanao
Associate Professor
Department of Applied Mechanics and Aerospace Engineering
Waseda University, Tokyo, 169-8555, Japan
E-mail: yanao@waseda.jp

in the Sun–Earth system. The method yields the novel family of transfers as well as those ending in direct capture orbits, under particular energetic and geometrical conditions.

Keywords Medium-energy transfer · Collision orbits · Levi–Civita regularization · Circular restricted three-body problem · Bicircular restricted four-body problem

1 Introduction

Low-energy transfers in multi-body systems have been extensively investigated to reduce the fuel consumption or to attain novel trajectory features. These transfers have been used in a number of space missions (Uesugi 1996; Burnett et al. 2003; Folta et al. 2012) and are proposed for future applications (Campagnola and Lo 2008). Typically, invariant manifolds emanating from Lagrange point orbits are used to analyze low-energy transfers in the restricted three-body problem, and to view ballistic capture from another perspective (Koon et al. 2001; Belbruno and Miller 1993). While low-energy solutions succeed in reducing the transfer cost, they often result in long transfer times. There is thus the need to search for intermediate solutions with shorter transfer times than low-energy transfers, at the expense of increasing their cost, which is supposed to be still lower than that of the classic patched-conics solutions. Solutions that reduced the transfer cost, with no penalty in transfer time, were found in Campagnola et al. (2014b,a)

In (Topputo 2013), a global search of trajectories from a low Earth orbit (circular, 167 km altitude) to a low lunar orbit (circular, 100 km altitude) was made, regardless of the orbit type (interior or exterior, high- or low-energy). In this analysis, a novel family of exterior transfers emerged. This family belongs to the Pareto set in a cost vs. time space, and possesses the intermediate features sought (see solutions (vii)–(ix) in Fig. 8 in Topputo (2013)). This class of "medium-energy" lunar transfers has four characteristics: 1) No portion of the transfer orbit can be related to the dynamics of the Lagrange points in the Sun–Earth system, 2) In a planar model, the angular momentum about the Moon at arrival is negative, i.e., the arrival orbit is retrograde, 3) The Kepler energy relative to the Moon at arrival is negative, i.e., the orbit experiences lunar ballistic capture, 4) The Jacobi energy in the Earth–Moon system is such that the forbidden regions vanish. This new family of solutions deserved an analysis to gain insights into its peculiar dynamics.

In the present work we investigate the dynamics of the lunar transfers in this medium-energy regime. At these energies, the invariant manifolds associated to the Lagrange point orbits cease to be well-behaved because of the close encounter with the smaller primary (the Moon in our case), which causes their Poincaré curves to open up, and cancels their separatrix role. Thus, studying the Lagrange point dynamics is not helpful in medium-energy levels as it is at low energies.

A way to recover this loss is considering the dynamics of singular collision orbits (or simply collision orbits), which pass through the center of the Moon. These orbits reveal to be an important backbone structure for the dynamics in the medium-energy regime. Complex structures, related to bounded and escape motion relative to the smaller primary, have been identified in several systems via collision orbits and Poincaré sections (Nagler 2005; Davis and Howell 2011; de

Assis and Terra 2012). Recent studies on stable sets behavior about the smaller primary have reported that a substantial portion of the weak stability boundaries is composed of collision orbits (Topputo and Belbruno 2009; Makó et al. 2010; Hyeraci and Topputo 2010; Sousa Silva and Terra 2012; Hyeraci and Topputo 2013; Luo et al. 2014; Luo and Topputo 2014), as well as of invariant manifolds emanating from Lyapunov orbits (Belbruno et al. 2010, 2013). Moreover, collision orbits have been proven to embed useful information in the context of mission design (Anderson and Lo 2005; Kirchbach et al. 2005; Anderson and Parker 2012, 2013).

By using Levi–Civita regularization (Lega et al. 2011), it is possible to treat lunar collision orbits as invariant objects in the Earth–Moon planar circular restricted three-body problem. We numerically reveal rich phase space structures including tube structures of lunar collision orbits for specified energy, and investigate the relationships between lunar collision orbits and two-body parameters at lunar capture (Kepler energy and angular momentum). In doing so, we give evidence that the retrograde ballistic capture orbits are bounded by lunar collision orbits, which may be thought as a valid substitute to invariant manifolds when designing medium-energy lunar transfers.

A method for constructing the novel exterior lunar transfers is spun-off from our analysis. This method implements the dynamics of the bicircular restricted four-body model and uses the patched restricted three-body models approximation (Koon et al. 2001); orbits inside the tube structure of lunar collision orbits in the Earth–Moon model are connected to those whose apogees lie in the second quadrant in the Sun–Earth model. By construction, this method works under particular conditions of Jacobi energy and orbit geometry. We obtain solutions whose time and cost are in-between those of high- and low-energy transfers. We also compute new medium-energy transfers leading to direct orbits around the Moon, so complementing the search in Topputo (2013).

The structure of the paper is as follows. In Section 2 the dynamical models are recalled along with their main features. In Section 3 the dynamics of collision orbits is studied, and their connection with the novel transfer orbits is discussed. The method to design novel lunar transfers is given in Section 4. Final remarks are given in Section 5.

2 Background

2.1 Planar Circular Restricted Three-Body Problem

The planar circular restricted three-body problem (PCR3BP) models the motion of a massless particle, P_3, under the gravitational influences of two primaries, P_1, P_2 of masses m_1, m_2, $m_1 > m_2$, which revolve in circular orbits around their barycenter. In the present study, we use the following normalized equations (see Szebehely (1967) for details)

$$\ddot{x} - 2\dot{y} = \frac{\partial \Omega_3}{\partial x}, \qquad \ddot{y} + 2\dot{x} = \frac{\partial \Omega_3}{\partial y}, \tag{1}$$

where

$$\Omega_3(x,y) = \frac{1}{2}(x^2+y^2) + \frac{1-\mu}{\sqrt{(x+\mu)^2+y^2}} + \frac{\mu}{\sqrt{(x-1+\mu)^2+y^2}} + \frac{1}{2}\mu(1-\mu), \quad (2)$$

is the effective potential, and $\mu = m_2/(m_1+m_2)$ is the mass parameter. The Jacobi integral is

$$J(x,y,\dot{x},\dot{y}) = 2\Omega_3(x,y) - (\dot{x}^2+\dot{y}^2), \quad (3)$$

and thus solutions lie on manifolds $\mathcal{J}(C) = \{(x,y,\dot{x},\dot{y}) \in \mathbb{R}^4 | J(x,y,\dot{x},\dot{y}) = C\}$ for some energy C. Projecting $\mathcal{J}(C)$ onto the configuration space (x,y) defines the Hill's regions, which confine the motion of P_3. Their topology changes at the values of $C = C_k$, corresponding to the Lagrange points L_k, $k = 1,\ldots,5$, see Figure 1. With $\mu = 0.0121506683$, we have $C_1 = 3.2003449098$, $C_2 = 3.1841641431$, and $C_3 = 3.0241502628$; $C_{4,5} = 3$, regardless of μ.

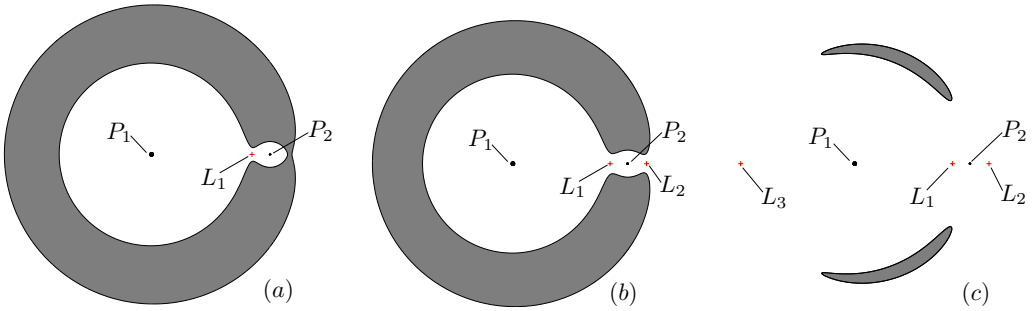

Fig. 1 Forbidden regions for varying energies. (a) $C_2 < C < C_1$; (b) $C_3 < C < C_2$; (c) $C_{4,5} < C < C_3$.

2.2 Planar Bicircular Restricted Four-Body Problem

The planar bicircular restricted four-body problem models the motion of a massless particle, P_3, under the gravitational influences of three massive bodies, P_0, P_1, P_2 of masses m_0, m_1, m_2, $m_0 > m_1 > m_2$, respectively. In the model, P_1 and P_2 revolve in circular orbits around their barycenter, and P_0 revolves in a circular orbit around the P_1–P_2 barycenter in the same orbital plane as P_3. In the present study, P_0 is the Sun, P_1 is the Earth, and P_2 is the Moon. The equations of motion are (Topputo 2013)

$$\ddot{x} - 2\dot{y} = \frac{\partial \Omega_4}{\partial x}, \qquad \ddot{y} + 2\dot{x} = \frac{\partial \Omega_4}{\partial y}, \quad (4)$$

where

$$\Omega_4(x,y,t) = \Omega_3(x,y) + \frac{\mu_s}{\sqrt{(x-a_s\cos\theta_s)^2+(y-a_s\sin\theta_s)^2}} - \frac{\mu_s}{a_s^2}(x\cos\theta_s + y\sin\theta_s), \quad (5)$$

where $\mu = m_2/(m_1 + m_2)$; μ_s is the mass of the Sun, a_s is the distance from the Earth–Moon barycenter to the Sun, and the phase angle of the Sun is $\theta_s(t) = \theta_{s,0} + \omega_s t$ for some initial $\theta_{s,0}$ at $t = 0$; ω_s is the relative angular velocity of the Sun. All the physical parameters used in the present study are in accordance with those reported in Table 3 in Topputo (2013).

3 Dynamics of Lunar Collision Orbits

3.1 Levi–Civita Regularization

In the present study, we analyze singular, collisional orbits passing through the center of the Moon in the Earth–Moon PCR3BP. We implement the Levi–Civita regularization about the Moon (see Lega et al. (2011))

$$x - 1 + \mu = {u_1}^2 - {u_2}^2, \quad y = 2u_1u_2, \quad \dot{x} = \frac{2(u_1u_3 - u_2u_4)}{{u_1}^2 + {u_2}^2}, \quad \dot{y} = \frac{2(u_2u_3 + u_1u_4)}{{u_1}^2 + {u_2}^2}, \tag{6}$$

where u_1, u_2 are regularized coordinates, u_3, u_4 are their derivatives with respect to the fictitious time s, respectively, $\mathrm{d}t = r\mathrm{d}s$, and r is the distance from the Moon. The equations of motion in regularized coordinates are

$$u_1' = u_3, \quad u_2' = u_4, \quad u_3' = \frac{1}{4}(a+b)u_1 + \frac{1}{4}cu_2, \quad u_4' = \frac{1}{4}(a-b)u_2 + \frac{1}{4}cu_1, \tag{7}$$

where

$$a = \frac{2(1-\mu)}{\sqrt{({u_1}^2 - {u_2}^2 + 1)^2 + 4{u_1}^2{u_2}^2}} - C + ({u_1}^2 - {u_2}^2 + 1 - \mu)^2 + 4{u_1}^2{u_2}^2 + \mu(1-\mu), \tag{8}$$

$$b = 8(u_2u_3 + u_1u_4) + 2({u_1}^2 + {u_2}^2)({u_1}^2 - {u_2}^2 + 1 - \mu) - \frac{2(1-\mu)({u_1}^2 - {u_2}^2 + 1)({u_1}^2 + {u_2}^2)}{[({u_1}^2 - {u_2}^2 + 1)^2 + 4{u_1}^2{u_2}^2]^{\frac{3}{2}}}, \tag{9}$$

$$c = 4u_1u_2({u_1}^2 + {u_2}^2) - 8(u_1u_3 - u_2u_4) - \frac{4(1-\mu)u_1u_2({u_1}^2 + {u_2}^2)}{[({u_1}^2 - {u_2}^2 + 1)^2 + 4{u_1}^2{u_2}^2]^{\frac{3}{2}}}. \tag{10}$$

Note that terms associated to $1/r$ are removed, thus Eq. (7) can handle the singularity $r \to 0$ in Eq. (1).

In this work, collision orbits are integrated starting with the initial conditions at the center of the Moon, $u_1 = u_2 = 0$, where the expression for the Jacobi constant (3) becomes (Broucke 1971)

$${u_3}^2 + {u_4}^2 = \frac{\mu}{2}, \tag{11}$$

Therefore, for a given μ, u_3 and u_4 can be parametrized with one angle, $\theta_c \in [0, 2\pi]$, and the initial conditions for collisional orbits are

$$u_1 = 0, \qquad u_2 = 0, \qquad u_3 = \sqrt{\frac{\mu}{2}}\cos\theta_c, \qquad u_4 = \sqrt{\frac{\mu}{2}}\sin\theta_c. \tag{12}$$

Note that while the initial conditions depend only on θ_c, the dynamical system Eq. (7) is further parametrized by a Jacobi constant C, which appears in Eq. (8).

3.2 Linear Stability Analysis

The null state ($\mathbf{u} = 0$) zeroes the right hand side of Eq. (7), therefore the origin is an equilibrium for the regularized dynamics. It is thus meaningful to study the linear stability for varying Jacobi energy. Linearizing Eq. (7) around the origin yields to two second-order identical, decoupled equations, each one having the form

$$v_1' = v_2, \quad v_2' = \frac{3(1-\mu) - C}{4} v_1, \tag{13}$$

where $v_1 = \{u_1, u_2\}$ and $v_2 = \{u_3, u_4\}$. The eigenvalues of Eq. (13) are

$$\lambda_1 = \frac{1}{2}\sqrt{3(1-\mu) - C}, \qquad \lambda_2 = -\frac{1}{2}\sqrt{3(1-\mu) - C}, \tag{14}$$

which indicate a bifurcation at $C^* = 3(1-\mu) = 2.9635479951$. More specifically, the system is unstable for $C < C^*$ and linearly marginally stable (purely imaginary eigenvalues) for $C > C^*$.

The linear analysis is assessed by integrating the initial conditions in Eq. (12) using the fully nonlinear, regularized equations of motion (7). In Case (a) we set $C_a > C^*$, whereas in Case (b) $C_b < C^*$. Backward integration is carried out from $t = 0$ to $t = -\pi$ for both cases. The results are shown in Fig. 2. As expected by the linear analysis, lunar collision orbits in Case (a) stay in the vicinity of the Moon, whereas those in Case (b) suddenly leave the Moon. A similar feature has been observed in Anderson and Lo (2005) in the Jupiter–Europa system.

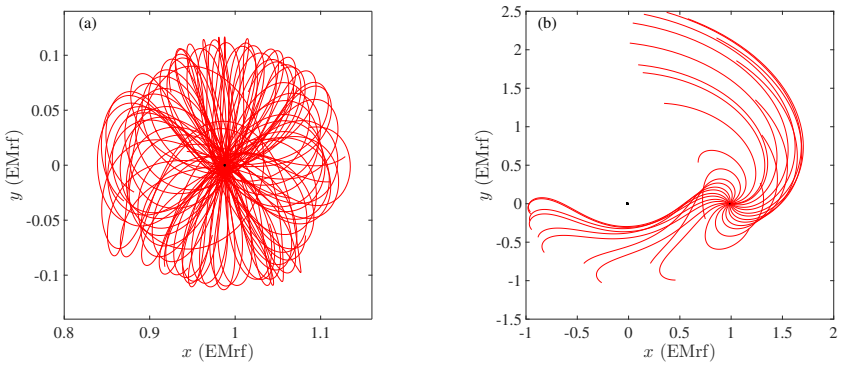

Fig. 2 Lunar collision orbits integrated from the center of the Moon backward in time within $[0, -\pi]$; Case (a): $C_a = 3.1720030296$, Case (b): $C_b = 2.9520030296$. 26 orbits are shown in each figure, whose initial conditions are evenly spaced in θ_c (see Eq. (12)). (In this Figure and in the remainder, EMrf abbreviates Earth–Moon rotating frame.)

3.3 Phase Space Structure of Lunar Collision Orbits

Figure 3 shows the cuts of the lunar collision orbits in Case (b) with a Poincaré section at $x = 0$, $\dot{x} > 0$ with (a) $y < 0$ and (b) $y > 0$. Note that the energy level

is such that forbidden regions vanish since $C_b < 3$. We include multiple crossings of the Poincaré section and stop integration if the trajectory is sufficiently far from the section, unless otherwise noted. We see that there are closed curves composed of lunar collision orbits in both figures, which indicate the existence of tube structures.

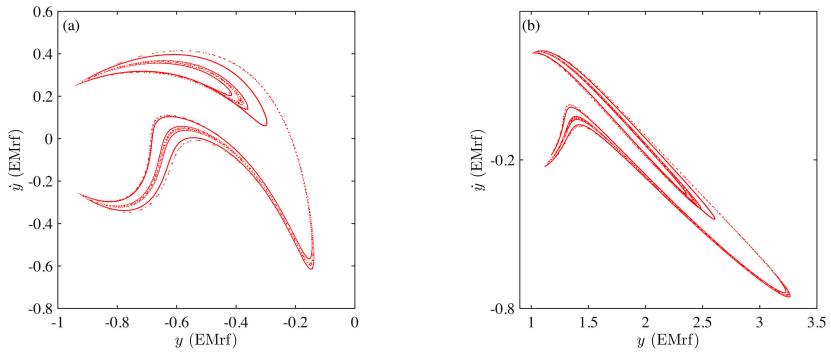

Fig. 3 The cuts of the lunar collision orbits in Case (b) on a Poincaré section at $x = 0$, $\dot{x} > 0$ and (a) $y < 0$, (b) $y > 0$. In both figures, 62832 collision orbits are integrated backward in time within $[0, -1000]$. There are 31610 intersections in (a) and 35495 in (b).

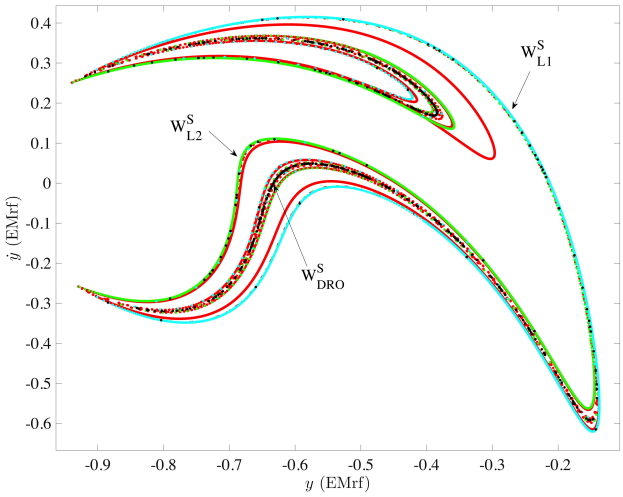

Fig. 4 The cuts of $W^S_{L_1}$ (cyan), $W^S_{L_2}$ (green), and W^S_{DRO} (black) on the same Poincaré section as in Fig. 3(a).

We then investigate a relationship between lunar collision orbits and invariant manifolds emanating from several unstable periodic orbits at the same energy (see Koon et al. (2011) for details on computing periodic orbits and their invariant manifolds). Fig. 4 shows the cuts of the stable manifolds emanating from the L_1 Lyapunov orbit $W^s_{L_1}$, L_2 Lyapunov orbit $W^s_{L_2}$, and period-3 distant retrograde orbit W^s_{DRO} (Capdevila et al. 2014; Mingotti et al. 2012) superimposed on the Poincaré section in Fig. 3(a). Note that at this energy level $W^s_{L_1}$ and $W^s_{L_2}$ do not form closed curves because of the close encounters to the Moon. Figure 4 indicates that lunar collision orbits have rich structures, and shadow the invariant manifolds of the unstable periodic orbits near the Moon.

Invariant manifolds of the period-3 Distant Retrograde Orbit (DRO) lie in the nested structures of lunar collision orbits. Since the period-3 DRO gives rise to homoclinic tangles (Wiggins 1991) that result in sticky motion around the secondary body (Scott and Spencer 2010), the nested structures could generate trajectories staying around the Moon for a long time.

In Fig. 5, we show four types of lunar collision orbits sampled from the Poincaré section in Fig. 3(a). The case of $y > 0$ (Fig. 3(b)) is qualitatively similar. Note that the lunar collision orbits near the nested structures (orbits (c) and (e)) exhibit looping behaviors around the Moon because of the sticky motion near invariant manifolds of the period-3 DRO. Fig. 5 also indicates that fast lunar collision orbits approaching the Moon without looping behaviors, such as the orbit in Fig. 5(b), may lie on the simple closed curve. This is confirmed in Section 3.4.

We also investigate the behavior of orbits taken across the lunar collision orbits in Fig. 3(b). In Fig. 6, orbits inside the closed curve, (d), (e), (f), may be regarded as the Type II (retrograde) flyby, whereas those outside, (b), (c), (g), (h), as the Type I (direct) flyby. This nomenclature refers to recently identified families of flybys in PCR3BP (Campagnola et al. 2012). The relationship between lunar collision orbits and the sign of angular momentum around the Moon is investigated in Section 3.5.

3.4 Looping Behavior of Collision Orbits

Although looping behavior is sometimes useful for mission trajectories (Uesugi 1996), it takes time of flight because of the non-straight motion. Since one of this work's motivations is the investigation of fast, medium-energy transfers, neglecting those lunar collision orbits exhibiting looping behavior eases our analysis.

Using Earth-centered polar coordinates (r, θ) it is possible to isolate and remove orbits exhibiting loops. Along one loop there are two points in which $\dot{\theta} = 0$, one having $\dot{r} > 0$ and the other $\dot{r} < 0$ (see Fig. 2(a) and Fig. 3 in Oshima and Yanao (2015) for details). Thus, we track $\dot{\theta} = 0$ events along lunar collision orbits, and if $\dot{r} > 0$ and $\dot{r} < 0$ occur in succession, the orbit is excluded from the analysis. Orbits that cross the abscissa of the Moon three times are not considered as well.

Fig. 7 shows the cuts of the lunar collision orbits in Fig. 3 when the two criteria above are applied. It is found that the simple lunar collision orbits (i.e., those with no loops) define closed curve on a Poincaré section. This is not trivial, and gives us a valid tool to replace invariant manifolds in the medium-energy regime. In Fig. 7 only the first intersection between the orbits and the surface of section is shown; this is also applied in the figures below, unless otherwise specified. We refer to γ

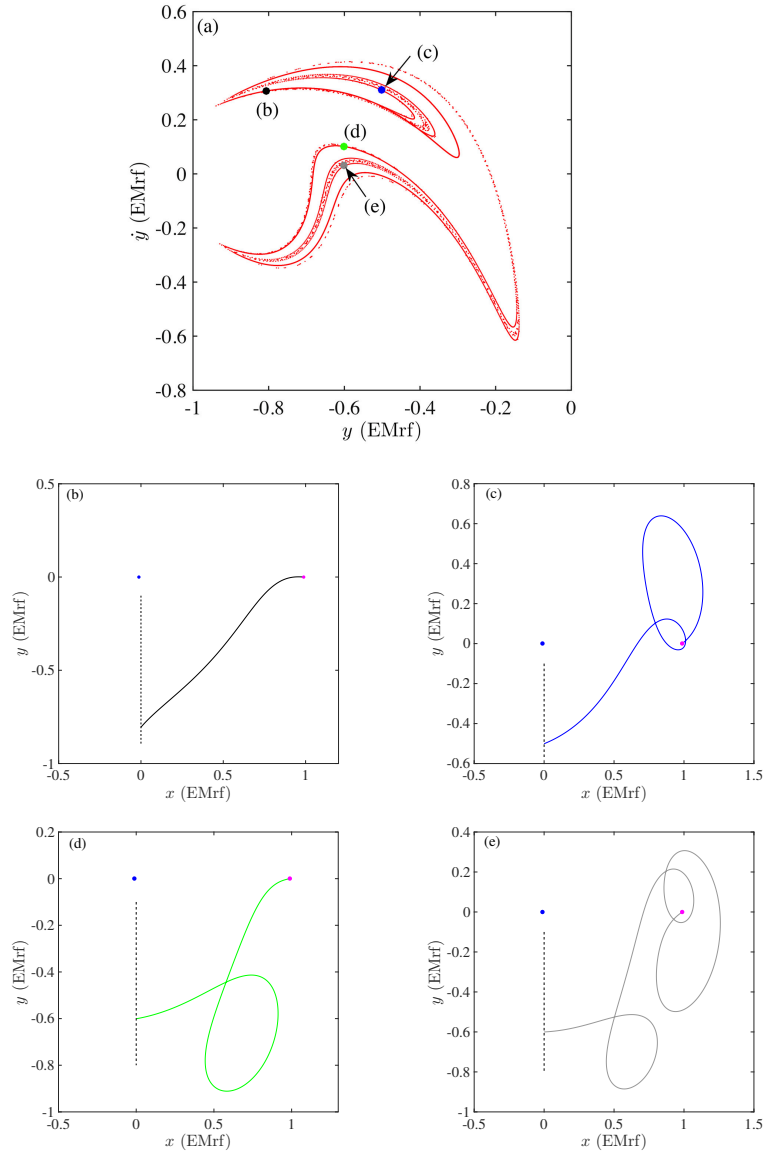

Fig. 5 Sample lunar collision orbits picked from Fig. 3(a). The blue spot is the Earth, the pink one is the Moon.

to indicate the curves having the same properties as those in Fig. 7. Note that point (b) in Fig. 5(a) belongs to γ_a in Fig. 7(a), whereas points (d), (e), and (f) in Fig. 6(a) are defined inside γ_b in Fig. 7(b).

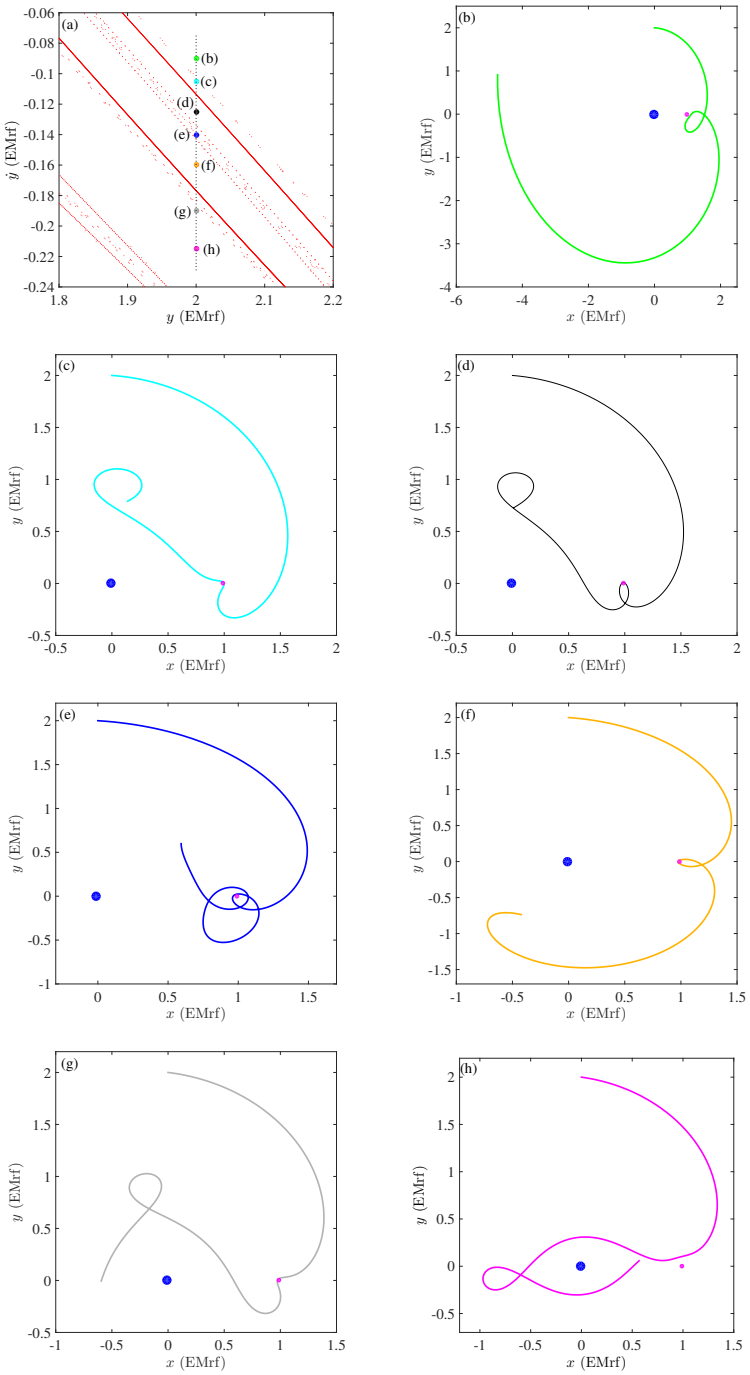

Fig. 6 Sample orbits taken across the closed curve in Fig. 3(b).

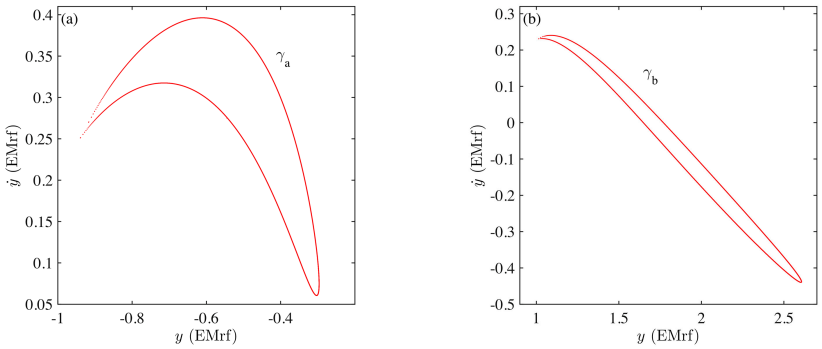

Fig. 7 The cuts of the lunar collision orbits in Fig. 3 once the looping orbits are removed; (a) $y < 0$, (b) $y > 0$.

3.5 Lunar Capture Portion of the Novel Transfer to the Moon

The new family of exterior transfers to the Moon (Pareto solutions (vii), (viii), (ix) in Fig. 8 in Topputo (2013)) has three distinct features in the lunar capture portion: 1) negative angular momentum (retrograde orbits), 2) negative Kepler energy (ballistic capture), and 3) medium energy regime (no forbidden regions).

Fig. 8 shows the projection of the reproduced Pareto solution (ix) obtained by integrating the orbital data (publicly available as supplemental material in Topputo (2013)) using the bicircular restricted four-body model, and the lunar collision orbits γ (red curves) computed in the PCR3BP.

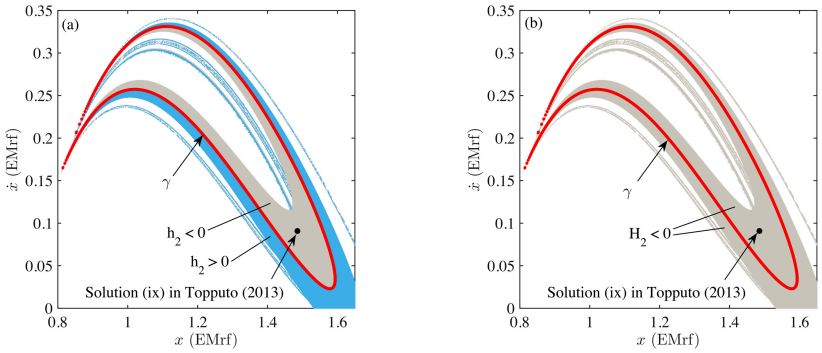

Fig. 8 The intersection of the reproduced Pareto solution (ix) in Topputo (2013) and the lunar collision orbits γ (red curve) on a Poincaré section with $C = 2.9947030296$, $y = 0.69612$, $\dot{y} < 0$. The location of the surface of section is chosen at the point where the Jacobi energy of the reference solution becomes nearly constant. The figures also show initial conditions that result in (a) positive angular momentum (cyan region) and negative angular momentum (grey region), and (b) negative Kepler energy (grey region) at the first Moon encounter at 100 km altitude or less after propagating from the Poincaré section in the Earth-Moon PCR3BP.

Fig. 8 also shows the initial conditions that result in low-altitude (below 100 km) close approaches at the Moon after propagating in the Earth-Moon PCR3BP. In particular, in Fig. 8(a) cyan points result in positive angular momentum (direct), and grey points result in negative angular momentum (retrograde). Fig. 8(b) shows the initial conditions generating orbits with negative Kepler energy (ballistic capture) at the first Moon encounter at 100 km altitude or less. Angular momentum, h_2, and Kepler energy, H_2, about the Moon in the Earth–Moon PCR3BP can be computed via (Topputo 2013)

$$h_2 = (x + \mu - 1)(\dot{y} + x + \mu - 1) - y(\dot{x} - y), \tag{15}$$

$$H_2 = \frac{1}{2}[(\dot{x} - y)^2 + (\dot{y} + x + \mu - 1)^2] - \frac{\mu}{r_2}, \tag{16}$$

where r_2 denotes the distance from the Moon.

The reference solution lies inside γ, which separates direct from retrograde lunar capture orbits. Retrograde orbits lie inside γ, whereas direct orbits lie outside γ, see Fig. 8(a). Note that there is a second complex structure inside γ; this is associated to orbits having looping behavior about the Moon. We see also that simple ballistic capture orbits reaching 100 km altitude at the Moon are defined near γ, see Fig. 8(b).

To sum up, results in Fig. 8 indicate that trajectories satisfying three distinct features in the lunar capture portion of the novel exterior transfer to the Moon in Topputo (2013), i.e., medium-energy, retrograde arrival, ballistic lunar capture, can be found inside γ on a Poincaré section. In this medium–energy regime, lunar collision orbits can replace invariant manifolds, which are not well-behaved in the low–energy regime.

4 Construction of the Novel Exterior Transfer to the Moon

We apply the analysis above to develop a method to qualitatively construct medium-energy, exterior transfers to the Moon. This is done by patching orbits inside γ and those whose apogees lie in the appropriate (second or fourth) quadrant (Miller 2003) in the Sun–Earth system. For this purpose we use the patched restricted three-body problem approximation (Koon et al. 2001) to derive initial guess solutions. These are later verified in the bicircular restricted four-body model.

The fourth interesting feature of the novel exterior transfers to the Moon is that they bounce at apogee far from Sun–Earth Lagrange points L_1 or L_2, i.e., the Sun–Earth Lagrange point dynamics is not utilized. In the Sun–Earth PCR3BP, we take $C_{SE} = C_1 + \varepsilon$, $\varepsilon > 0$, and focus on the second quadrant around the Earth. Note that C_{SE} corresponds to closed forbidden regions at both L_1 and L_2. This proves that the Sun–Earth Lagrange point dynamics is not used.

Fig. 9 shows a portion of the zero velocity curve (green) and the boundaries of the second quadrant (black and cyan). We consider that initial conditions with $C = C_{SE}$ on the green curve ($\dot{x} = 0$, $\dot{y} = 0$), black line ($x = 1 - \mu$, $\dot{y} = 0$), and cyan line ($y = 0$, $\dot{x} = 0$) represent the boundaries of trajectories bouncing in the second quadrant with $C = C_{SE}$.

We then propagate these initial conditions forward in time using the equations of motion of the Sun–Earth PCR3BP. Since we seek bounces at apogees, not at

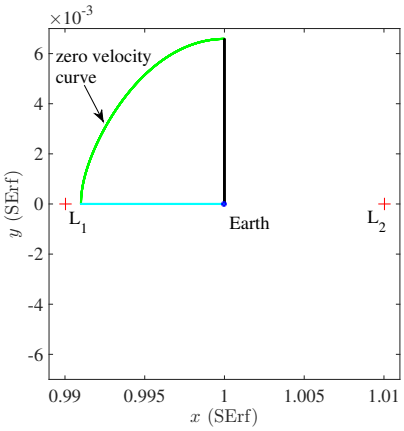

Fig. 9 A portion of the zero velocity curve (green) and the boundaries of orbits bouncing in the second quadrant (black, cyan); $C_{SE} = 3.0009030034$.

perigees, we only integrate the initial conditions satisfying $\ddot{r}_E < 0$, where $r_E = [(x - 1 + \mu)^2 + y^2]^{1/2}$ is the distance from the Earth. Note that $\dot{r}_E = 0$, $\ddot{r}_E < 0$ is the condition for apogees. We stop integration at a Poincaré section $y = -0.00102782085$, which corresponds to a Poincaré section $y = 0.4$ in the Earth–Moon rotating frame with the phase of the Sun $\theta_S = 0$. These intersections are transformed into the Earth–Moon system (Koon et al. 2011) with $\theta_S = 0$ (see Fig. 10 that uses the same color code). For computation of the trajectories in the portion of the Earth–Moon PCR3BP, we propagate the lunar collision orbits with $C_{EM} = 2.9920030296$ using the regularized equations of motion Eq. (7) backward in time to the same Poincaré section $y = 0.4$ in the Earth–Moon rotating frame and isolate γ (red in Fig. 10).

The result of superposition in Fig. 10(a) exhibits an intersection of γ and the region of trajectories with apogees in the second quadrant. Thus, the patched three-body technique (Koon et al. 2001) indicates that the intersecting region is of potential interest.

We then perform two-dimensional grid search, i.e., propagate forward and backward in time from the vicinity of the intersection on the Poincaré section: $1.2 \leq x \leq 1.6$ and $-0.22 \leq \dot{x} \leq 0.11$ with $C = C_{EM}$ and $\theta_S = 0$, using the bicircular restricted four-body model in the Earth–Moon rotating frame. By this search, we could find solutions reaching the predefined boundary conditions: 100 km altitude at the Moon and 167 km altitude at the Earth. Point P, the black dot in Fig. 10, is the solution having the lowest cost.

Fig. 11 shows the trajectory propagated from P forward and backward in time using the bicircular restricted four-body model and shown in the (a) Earth–Moon rotating frame and (b) Sun–Earth rotating frame. For this solution, the total time of flight is 66.25 days and cost is 3820 m/s, which are similar values of the focused Pareto solutions (vii), (viii), (ix) in Topputo (2013). Moreover, the obtained solution reproduces the distinct four features of the novel exterior transfers; dynamics of Lagrange points in the Sun–Earth system is not utilized, final angular momentum around the Moon is negative ($h_2 = -0.0107$), final Kepler

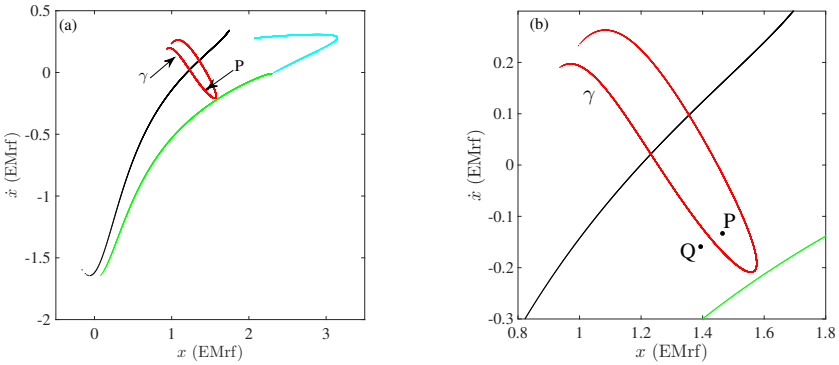

Fig. 10 Superposition of γ (red) and the trajectories integrated from the boundaries in Fig. 9. Point P (black dot) is the solution with the lowest cost. (b) is a particular of (a).

energy around the Moon is negative ($H_2 = -0.02427$), and medium energy ($C_{EM} < 3$, no forbidden regions).

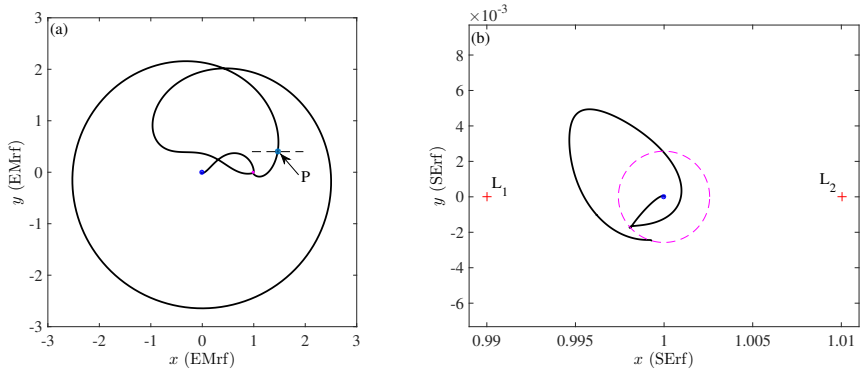

Fig. 11 The transfer trajectory leading to a retrograde orbit around the Moon obtained by propagating P forward and backward in time. (a) Earth–Moon rotating frame, (b) Sun–Earth rotating frame. (The dashed line at $y = 0.4$ in Fig. 11(a) represents the surface of section on which Fig. 10 is achieved.)

4.1 Direct medium-energy solutions

In Topputo (2013), families of transfers usually came in pairs, with each direct-approach family shadowing the retrograde-approach one. The retrograde solutions typically improve on the cost of the direct solutions. In fact, while the velocity in the rotating frame is almost fixed for a given r and C (see Campagnola and Russell (2010)), when computing the orbit insertion costs, retrograde solutions benefit from the relative velocity of the reference frame, while direct solutions are

penalized by the same amount. The retrograde family discussed in the present paper, however, was not paired by a direct family in Topputo (2013).

We used our method to compute a new family leading to direct orbits around the Moon and found them from outside γ on the Poincaré section (point Q in Fig. 10(b)). Fig. 12 shows the obtained direct solution with the lowest cost shown in (a) the Earth–Moon rotating frame and (b) the Sun–Earth rotating frame. The total time of flight is 65.98 days and the sum of fuel consumption is 3859 m/s. We confirm that the obtained direct solution also possesses the distinct features of the novel exterior transfers except for the sign of the angular momentum.

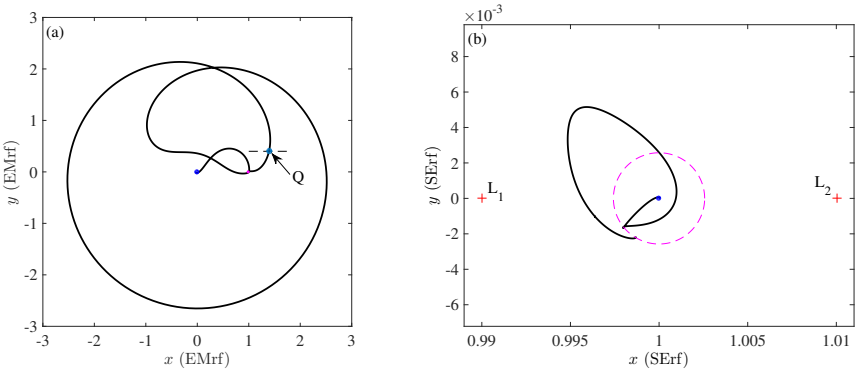

Fig. 12 The obtained transfer trajectory leading to a direct orbit around the Moon. (a) Earth–Moon rotating frame, (b) Sun–Earth rotating frame.

5 Conclusions

The present study analyzes medium-energy dynamics based on collision orbits with the Moon in the Earth–Moon planar circular restricted three-body problem. We have revealed rich phase-space structures of lunar collision orbits and investigated the relationships between lunar collision orbits and two-body parameters at lunar capture (Kepler energy and angular momentum) in the medium-energy regime.

The analysis is applied to develop a method for constructing the novel exterior transfer to the Moon previously found by Topputo (2013). The proposed method works in the medium-energy regime once geometrical conditions on the collision are satisfied. The rationale is exploiting information of the tube structures of lunar collision orbits and boundaries of bounces in appropriate quadrant around the Earth at apogees. By this method, we have constructed trajectories of the same family of the novel lunar transfers, and also found medium-energy transfers leading to direct orbits around the Moon in the bicircular restricted four-body model.

Acknowledgements This study has been partially supported by Grant-in-Aid for JSPS Fellows No. 15J07090, and by JSPS Grant-in-Aid No. 26800207.

References

Anderson, R. L., Lo, M. W.: Virtual exploration by computing global families of trajectories with supercomputers. 15th AAS/AIAA Space Flight Mechanics Meeting, AAS 05-220, Copper Mountain, CO, (2005)

Anderson, R. L., Parker, J. S.: Survey of ballistic transfers to the lunar surface. J. Guid. Control Dyn. **35**, 1256–1267 (2012). doi:10.2514/1.54830

Anderson, R. L., Parker, J. S.: Comparison of low-energy lunar transfer trajectories to invariant manifolds. Celest. Mech. Dyn. Astr. **115**, 311–331 (2013). doi:10.1007/s10569-012-9466-3

Belbruno, E., Miller, J.: Sun-perturbed Earth-to-Moon transfers with ballistic capture. J. Guid. Control Dyn. **16**, 770–775 (1993). doi:10.2514/3.21079

Belbruno, E., Gidea, M., Topputo, F.: Weak stability boundary and invariant manifolds. SIAM J. Appl. Dyn. Syst. **9**, 1061–1089 (2010). doi:10.1137/090780638

Belbruno, E., Gidea, M., Topputo, F.: Geometry of weak stability boundaries. Qualit. Theory of Dyn. Syst. **12**, 53–66 (2013). doi:10.1007/s12346-012-0069-x

Broucke, B.: Periodic collision orbits in the elliptic restricted three-body problem. Celestial Mechanics **3**, 461–477 (1971). doi:10.1007/BF01227792

Burnett, D. S., Barraclough, B. L., Bennett, R., Neugebauer, M., Oldham, L. P., Sasaki, C. N., Sevilla, D., Smith, N., Stansbery, E., Sweetnam, D., Wiens, R. C.: The GENESIS discovery mission: Return of solar matter to the Earth. Space Sci. Rev. **105**, 509–534 (2003). doi:10.1023/A:1024425810605

Campagnola, S., Lo, M. W.: BepiColombo gravitational capture and the elliptic, restricted three-body problem. Proceedings in Applied Mathematics and Mechanics **7**, 1030905–1030906 (2008). doi:10.1002/pamm.200700330

Campagnola, S., Russell, R. P.: Endgame problem part 2: Multi-body technique and T-P graph. J. Guid. Control Dyn. **33**, 476–486 (2010). doi:10.2514/1.44290

Campagnola, S., Skerritt, P., Russell, R. P.: Flybys in the planar, circular, restricted, three-body problem. Celest. Mech. Dyn. Astr. **113**, 343–368 (2012). doi:10.1007/s10569-012-9427-x

Campagnola, S., Boutonnet, A., Schoenmaekers, J., Grebow, D. J., Petropoulos, A.E.: Tisserand-Leveraging Transfer. J. Guid. Control Dyn. **37**, 1202–1210 (2014). doi:10.2514/1.62369

Campagnola, S., Buffington, B. B., Petropoulos, A.E.: Jovian tour design for orbiter and lander missions to Europa. Acta Astronaut. **100**, 68–81 (2014). doi:10.1016/j.actaastro.2014.02.005

Capdevila, L., Guzzetti, D., Howell, K.: Various transfer options from Earth into distant retrograde orbits in the vicinity of the Moon. 24th AAS/AIAA Space Flight Mechanics Meeting, AAS 14-467, Santa Fe, NM, (2014)

Davis, D. C., Howell, K. C.: Trajectory evolution in the multi-body problem with applications in the Saturnian system. Acta Astronaut. **69**, 1038–1049 (2011). doi:10.1016/j.actaastro.2011.07.007

De Assis, S. C., Terra, M. O.: Escape dynamics and fractal basin boundaries in the planar Earth–Moon system. Celest. Mech. Dyn. Astr. **120**, 105–130 (2014). doi:10.1007/s10569-014-9567-2

Folta, D. C., Woodard, M., Howell, K., Patterson, C., Schlei, W.: Applications of multi-body dynamical environments: The ARTEMIS transfer trajectory design. Acta Astronaut. **73**, 237–249 (2012). doi:10.1016/j.actaastro.2011.11.007

Hyeraci, N., Topputo, F.: Method to design ballistic capture in the elliptic restricted three-body problem. J. Guid. Control Dyn. **33**, 1814–1823 (2010). doi:10.2514/1.49263

Hyeraci, N., Topputo, F.: The role of true anomaly in ballistic capture. Celest. Mech. Dyn. Astr. **116**, 175–193 (2013). doi:10.1007/s10569-013-9481-z

Koon, W. S., Lo, M. W., Marsden, J. E., Ross, S. D..: Low energy transfer to the Moon. Celest. Mech. Dyn. Astr. **81**, 63–73 (2001). doi:10.1023/A:1013359120468

Koon, W. S., Lo, M. W., Marsden, J. E., Ross, S. D..: Dynamical Systems, the Three-Body Problem and Space Mission Design. Marsden Books, Wellington (2011)

Lega, E., Guzzo, M., Froeschlé, C.: Detection of close encounters and resonances in three-body problems through Levi–Civita regularization. MNRAS **418**, 107–113 (2011). doi:10.1111/j.1365-2966.2011.19467.x

Luo, Z.-F., Topputo, F., Bernelli-Zazzera, F., Tang, G.-J.: Constructing ballistic capture orbits in the real solar system model. Celest. Mech. Dyn. Astr. **120**, 433–450 (2014).

doi:10.1007/s10569-014-9580-5
Luo, Z.-F., Topputo, F.: Analysis of ballistic capture in Sun–planet models. Adv. Space. Res. **56**, 1030-1041 (2015). doi:10.1016/j.asr.2015.05.042
Makó, Z., Szenkovits, F., Salamon, J., Oláh-Gál, R.: Stable and unstable orbits around Mercury. Celest. Mech. Dyn. Astr. **108**, 357–370 (2010). doi:10.1007/s10569-010-9309-z
Miller, J.: Lunar transfer trajectory design and the four-body problem. 13th AAS/AIAA Space Flight Mechanics Meeting, AAS 03-144, At Ponce, Puerto Rico, (2003)
Mingotti, G., Topputo, F., Bernelli-Zazzera, F.: Transfers to distant periodic orbits around the Moon via their invariant manifolds. Acta Astr. **79**, 20–32 (2012). doi:10.1016/j.actaastro.2012.04.022
Nagler, J.: Crash test for the restricted three-body problem. Phys. Rev. E **71**, 06227 (2005). doi:10.1103/PhysRevE.71.026227
Oshima, K., Yanao, T.: Jumping mechanisms of Trojan asteroids in the planar restricted three- and four-body problems. Celest. Mech. Dyn. Astr. **122**, 53–74 (2015). doi:10.1007/s10569-015-9609-4
Scott, C. J., Spencer, C. D.: Calculating transfer families to peroidic distant retrograde orbits using differential correction. J. Guid. Control Dyn. **33**, 1592–1605 (2010). doi:10.2514/1.47791
Sousa Silva, P. A., Terra, M. O.: Applicability and dynamical characterization of the associated sets of the algorithmic weak stability boundary in the lunar sphere of influence. Celest. Mech. Dyn. Astr. **113**, 141–168 (2012). doi:10.1007/s10569-012-9409-z
Szebehely, V..: Theory of Orbits: The Restricted Problem of Three Bodies. Academic Press Inc, New York (1967)
Topputo, F., Belbruno, E.: Computation of weak stability boundaries: Sun-Jupiter system. Celest. Mech. Dyn. Astr. **105**, 3–17 (2009). doi:10.1007/s10569-009-9222-5
Topputo, F.: On optimal two-impulse Earth–Moon transfers in a four-body model. Celest. Mech. Dyn. Astr. **117**, 279–313 (2013). doi:10.1007/s10569-013-9513-8
Uesugi, K.: Results of the MUSES-A "HITEN" mission. Adv. Space. Res. **18**, 69-72 (1996). doi:10.1016/0273-1177(96)00090-7
von Kirchbach, C., Zheng, H., Aristoff, J., Kavanagh, J., Villac, B. F., Lo, M. W.: Trajectories leaving a sphere in the restricted 3-body problem. 15th AAS/AIAA Space Flight Mechanics Meeting, AAS 05-221, Copper Mountain, CO, (2005)
Wiggins, S.: Chaotic Transport in Dynamical Systems. Springer-Verlag, New York (1991)